Band-gap renormalization in quantum wire systems: dynamical correlations and multi-subband effects

J. Phys.: Condens. Matter **12** (2000) 2031–2042. Printed in the UK PII: S0953-8984(00)08284-9

Band-gap renormalization in quantum wire systems: dynamical correlations and multi-subband effects

K Güven†, B Tanatar† and C R Bennett‡

† Department of Physics, Bilkent University, Bilkent, 06533 Ankara, Turkey
‡ Department of Physics, University of Essex, Colchester CO4 3SQ, UK

Received 30 September 1999, in final form 2 November 1999

Abstract. We study the band-gap renormalization in a model semiconductor quantum wire due to the exchange–correlation effects among the charge carriers. We construct a two-subband model for the quantum wire, and employ the GW-approximation to obtain the renormalized quasi-particle energies at the optical band edge. The renormalization is calculated as a function of electron–hole plasma density and the wire radius. Our results show that the very presence of the second subband affects the renormalization process even in the absence of occupation by the carriers. We compare the fully dynamical random-phase approximation results to the quasi-static case in order to emphasize the dynamical correlation effects. Effects of electron–phonon interaction within the two-subband model are also considered.

1. Introduction

The motivation supplied by the enormous success of two-dimensional (2D) structures both in fundamental research and device applications has driven the trend to continue to reduce the dimensions of the electron systems. Indeed, in the last two decades, much effort has been devoted to reducing the dimensionality towards 1D and 0D in the semiconductor structures. Since the first suggestion by Sakaki [1] and the experimental realization by Petroff *et al* [2], quasi-one-dimensional (Q1D) semiconductor structures have constituted an extensive research area. Electrons in quantum wires are considered as a realization of one-dimensional Fermi gas. Progress in the fabrication techniques such as molecular beam epitaxy and lithographic deposition have made possible the production of such Q1D systems [3], where one-dimensional electron dynamics can be studied in a controlled and quantitative manner. This, in turn, acts as a feedback to theoretical studies.

In this work, we investigate the many-body correlation effects in a dense electron–hole plasma on the optical band-gap of a semiconductor quantum wire. Under intense laser excitation, such a two-component plasma with densities well above the Mott transition regime can be formed. Typical densities realized in experimental studies [4, 5] vary in the range $N = 10^5$–10^7 cm^{-1}. Because of the exchange–correlation effects, the properties of the system based on a single-particle approach get 'renormalized'. One important feature is the density-dependent shrinkage of the fundamental band-gap of the semiconductor. As a substantial level of carrier population may be induced by optical excitation, the renormalized band-gap can affect the excitation process in turn and lead to optical nonlinearities [6]. Band-gap renormalization as well as various optical properties of the Q1D electron–hole systems have been studied [7–14],

0953-8984/00/092031+12$30.00

similarly to the case for bulk (3D) and quantum well (2D) semiconductors [15–17] where generally good agreement with the corresponding measurements [18–21] is found.

Density dependence of the BGR in Q1D systems was first considered theoretically by Benner and Haug [7] within the quasi-static approximation. Hu and Das Sarma [9] calculated the BGR neglecting the hole population and considering the electron plasma confined in the lowest conduction subband only. Tanatar [10] studied the BGR due to a Q1D electron–hole plasma by employing the quasi-static approximation. Despite these intensive theoretical efforts, recent experimental studies reflect the fact that the quantitative assessment of the BGR is still an unsettled issue. Theoretical results usually predict rather large BGR values [9, 10] ($\sim$20 meV), whereas in some applications [19–22] the simple Hartree–Fock approximation already yields quantitative agreement with experiments. Part of the difficulty in discerning the BGR is associated with the way in which it is extracted from the data. It probably depends sensitively on the model that one uses in the analysis of photoluminescence (PL) or excitation photoluminescence (PLE) spectra.

The chief aim of our investigation is to employ the standard perturbation theory methods to calculate the BGR in quantum wires and compare with various approximations. In particular we stress the importance of including the dynamical correlation effects and the subband structure to reproduce the trends in measured BGR.

The rest of this paper is organized as follows. In the next section we present the model of a multi-subband quantum wire and lay out the theoretical description of the self-energy calculations in various approximations. In section 3 we illustrate the results of our calculations and discuss them in relation to other works. We conclude with a brief summary in section 4.

2. Theoretical background

2.1. Model

We choose our model wire [22] with a cylindrical cross-section of radius R_0 and an infinite potential barrier. The subband structure of the Q1D system is determined by the confinement potential. When the Fermi energy E_F exceeds the difference between the subband energy levels, the second subband starts to be populated. In the present model at zero temperature, this occurs when $NR_0 \sim 6/\pi$. For a typical wire radius of 100 Å, the corresponding density for the onset of second-subband population is $N \sim 1.9 \times 10^6$ cm^{-1}, which can easily be attained in experiment. The Fermi wavenumber k_F is related to the density of electron–hole plasma for one-subband population by $N = 2k_F/\pi$. The Coulomb interaction matrix elements can be calculated from

$$V_{klmn}(q) = \frac{e^2}{\epsilon_0} \int \mathrm{d}\boldsymbol{r} \int \mathrm{d}\boldsymbol{r}' \; \psi_k^*(\boldsymbol{r})\psi_l^*(\boldsymbol{r}') \frac{\mathrm{e}^{\mathrm{i}q(z-z')}}{|\boldsymbol{r}-\boldsymbol{r}'|} \psi_m(\boldsymbol{r})\psi_n(\boldsymbol{r}') \tag{1}$$

where $\psi_n(\boldsymbol{r})$ are the subband wavefunctions and ϵ_0 is the background dielectric constant. The above matrix element can be interpreted as the scattering of two carriers from initial subbands k, l into subbands m, n, respectively. In this respect, V_{1111} is an intra-subband interaction with all carriers remaining in the first subband, V_{1221} describes the scattering of two carriers in first and second subbands respectively, where no inter-subband transitions are induced, and V_{1122} is an inter-subband interaction in which both carriers are scattered from the first subband to the second subband. Interactions that couple the inter-subband and intra-subband modes are not allowed in the symmetric confinement, due to the definite parity of the envelope functions. This can be formulated as $V_{klmn} = 0$, if $k + l + m + n =$ odd number, and the matrix elements remain the same under the permutation of the first and second pair of indices among themselves and among each other [24]. Gold and Ghazali [23] presented analytical results for the matrix

elements in a cylindrical confinement, by employing approximate wavefunctions. For our two-subband formalism, the relevant matrix elements are given by [23]

$$V_{1111} = \frac{2e^2}{\epsilon_0}\frac{2304}{x^6}\left[\frac{1}{6} - \frac{x^2}{96} + \frac{x^4}{640} - I_3(x)K_3(x)\right] \tag{2a}$$

$$V_{1212} = \frac{2e^2}{\epsilon_0}\frac{18\,432}{x^6}\left[\frac{1}{8} - \frac{x^2}{240} + \frac{x^4}{3840} - I_4(x)K_4(x)\right] \tag{2b}$$

$$V_{1122} = \frac{2e^2}{\epsilon_0}\frac{9216}{x^6}\left[\frac{1}{24} - \frac{x^2}{960} + \frac{x^4}{3840} - K_3(x)\left(I_3(x) - \frac{6}{x}I_4(x)\right)\right] \tag{2c}$$

$$V_{2222} = \frac{2e^2}{\epsilon_0}\frac{36\,864}{x^6}\left[\frac{3}{2x^2} + \frac{1}{15} - \frac{x^2}{960} + \frac{x^4}{13\,440} - \left(I_3(x) - \frac{6}{x}I_4(x)\right)\left(K_3(x) + \frac{6}{x}K_4(x)\right)\right] \tag{2d}$$

where $x = qR_0$, and $I_n(x)$ and $K_n(x)$ denote the modified Bessel functions of the first and second kind, respectively. For numerical purposes, asymptotic forms may be useful for low q-values. Within this simple mathematical two-subband model, we also assume that only one kind of electron and one kind of hole with parabolic isotropic dispersions exist. This should be an adequate approximation for calculating the renormalization at the band edges, especially for GaAs.

2.2. Self-energy

This section presents the explicit expressions for the self-energy of electrons and holes in a multi-subband quantum wire. We employ the equilibrium formulation developed previously [9, 17], which is based on the so-called GW-approximation for the self-energy. This represents the self-energy operator by its leading term in the iterative expansion in powers of the dynamically screened electron–electron (hole) interaction. The assumption of equilibrium between the electrons and holes is adequate since the intra-band relaxation rates are typically much larger than the inter-band recombination and relaxation rates. By using the fully dynamical RPA dielectric function for the two-component plasma, we expect to retain the dynamical correlations properly within this scheme. For a multi-subband system, the renormalization of the ith subband is given by the sum of self-energies of electrons and holes evaluated at the subband edge (we take Planck's constant $\hbar$ and the Boltzmann constant k_B equal to unity throughout the formalism):

$$\Delta_i = \sum_\lambda \mathrm{Re}\ \Sigma^\lambda_{ii}(k = 0, \omega = \xi^{\lambda,i}_{k=0}) \tag{3}$$

where

$$\xi^{\lambda,j}_k = \frac{k^2}{2m^*_\lambda} + E^\lambda_j$$

denotes the quasi-particle energy of the λ-species (e, h) in jth subband of energy E^λ_j with respect to chemical potential μ^λ. The self-energy in the GW-approximation [25] which is attached to the external electron (hole) lines from subband i and j is given by

$$\Sigma^\lambda_{ij}(k, \omega) = \mathrm{i}\sum_l 2T \sum_{\omega_m > 0}\int \frac{\mathrm{d}q}{2\pi}\ W_{illj}(q, \omega_m)G^0_{ll}(k + q, \omega + \omega_m) \tag{4}$$

where the first sum is over the subbands, and the second sum represents the sequence of Matsubara frequencies $\omega_m = (2m + 1)\pi T$. G^0_{ij} is the noninteracting Green's function

$$G^0_{ij}(k, \mathrm{i}\omega_m) = \frac{\delta_{ij}}{\mathrm{i}\omega_m - \xi_k - E_j}. \tag{5}$$

The screened interaction matrix elements W_{illj} can be obtained from the matrix equation

$$\widetilde{W} = \widetilde{\varepsilon}^{-1}\widetilde{V}. \tag{6}$$

The components of the dielectric matrix $\widetilde{\varepsilon}$ are given in the RPA as

$$\varepsilon_{klmn}(q,\omega) = \delta_{km}\delta_{ln} - V_{klmn}(q)\Pi_{mn}(q,\omega) \tag{7}$$

where, for a two-component plasma, $\Pi_{mn} = \Pi^{e}_{mn} + \Pi^{h}_{mn}$ is the sum of the noninteracting polarizability functions of electrons and holes. The noninteracting polarizability is expressed as

$$\Pi^{\lambda}_{mn}(q,\omega) = 2\int \frac{\mathrm{d}k}{2\pi}\,\frac{n_F(\xi^{\lambda,m}_{k+q}) - n_F(\xi^{\lambda,n}_{k})}{\xi^{\lambda,m}_{k+q} - \xi^{\lambda,n}_{k} - \omega}. \tag{8}$$

This formulation yields the following screened interaction matrix $\widetilde{W}$ [9]:

$$\begin{bmatrix} \dfrac{V_{1111}(1 - V_{2222}\Pi_{22}) + V^2_{1122}\Pi_{22}}{\varepsilon_{intra}} & \dfrac{V_{1122}}{\varepsilon_{intra}} & 0 & 0 \\ \dfrac{V_{1122}}{\varepsilon_{intra}} & \dfrac{V_{2222}(1 - V_{1111}\Pi_{11}) + V^2_{1122}\Pi_{11}}{\varepsilon_{intra}} & 0 & 0 \\ 0 & 0 & \dfrac{V_{1212}}{\varepsilon_{inter}} & \dfrac{V_{1212}}{\varepsilon_{inter}} \\ 0 & 0 & \dfrac{V_{1212}}{\varepsilon_{inter}} & \dfrac{V_{1212}}{\varepsilon_{inter}} \end{bmatrix}.$$

In this block-diagonal form, the upper block represents the intra-subband interaction, whereas the lower block includes the inter-subband terms. Similarly, the dielectric function has the intra-subband and inter-subband components given respectively as

$$\begin{aligned}\varepsilon_{intra}(q,\omega) = {} & [1 - V_{1111}(q)\Pi_{11}(q,\omega)]\,[1 - V_{2222}(q)\Pi_{22}(q,\omega)] \\ & - V^2_{1122}(q)\Pi_{11}(q,\omega)\Pi_{22}(q,\omega)\end{aligned} \tag{9}$$

and

$$\varepsilon_{inter}(q,\omega) = 1 - V_{1212}(q)\,[\Pi_{12}(q,\omega) + \Pi_{21}(q,\omega)]\,. \tag{10}$$

In evaluating the self-energy, one usually decomposes it into screening-independent exchange and correlation terms (see e.g. Hu and Das Sarma [9]). An alternative way to proceed is to make this decomposition into so-called screened exchange and Coulomb-hole terms [26]:

$$\mathrm{Re}\,\Sigma_{ii} = \mathrm{Re}\,\Sigma^{sx}_{ii} + \mathrm{Re}\,\Sigma^{Ch}_{ii} \tag{11}$$

so that

$$\mathrm{Re}\,\Sigma^{sx(\lambda)}_{ii}(0, E^{\lambda}_{i}) = -\sum_{j}\int \frac{\mathrm{d}q}{2\pi}\,\mathrm{Re}[W_{ijji}(q, E^{\lambda}_{i} - \xi^{\lambda,j}_{q})]n_F(\xi^{\lambda,j}_{q}) \tag{12}$$

and

$$\begin{aligned}\mathrm{Re}\,\Sigma^{Ch(\lambda)}_{ii}(0, E^{\lambda}_{i}) = {} & -\sum_{j}\int \frac{\mathrm{d}q}{2\pi}\,\mathrm{Re}[W_{ijji}(q, E^{\lambda}_{i} - \xi^{\lambda,j}_{q}) - V_{ijji}(q)]n_B(\xi^{\lambda,j}_{q} - E^{\lambda}_{i}) \\ & + \sum_{j} 2T \sum_{\omega_m > 0}\int \frac{\mathrm{d}q}{2\pi}\,\frac{\xi^{\lambda,j}_{q} - E^{\lambda}_{i}}{\omega^2_m + (\xi^{\lambda,j}_{q} - E^{\lambda}_{i})^2}[W_{ijji}(q, \mathrm{i}\omega_m) - V_{ijji}(q)]\end{aligned} \tag{13}$$

where the two terms in the Coulomb-hole part are called the residue and line terms, respectively [26]. The above expressions (equations (12), (13)) represent the fully dynamical, temperature-dependent self-energy in a two-subband system. To assess the importance of the dynamical

correlations, a comparison with the quasi-static approximation should be made; we present such an approximation below.

The quasi-static approximation [15] amounts to neglecting the recoil effects relative to the plasma frequency in the full frequency-dependent expressions, and replaces the dielectric function by its static value in the final expressions. Note that the 'quasi-static' approximation is different to the simple static approximation which arises if the screened interaction in equation (4) is replaced *a priori* by its static value. This scheme totally neglects the Coulomb-hole energy and, as noted in the literature [15], can lead to serious errors. In the quasi-static limit (i.e. $W_{ijji}(q, \omega \to 0)$), only the fractional expression in the line term (equation (12)) depends on the Matsubara frequency, and that sum can be evaluated as follows:

$$2T \sum_{\omega_m > 0} \frac{\xi_q^{\lambda,j} - E_i^\lambda}{\omega_m^2 + (\xi_q^{\lambda,j} - E_i^\lambda)^2} = \frac{1}{2} \tanh\left(\frac{\xi_q^{\lambda,j} - E_i^\lambda}{2T} \right). \tag{14}$$

Hence,

$$\mathrm{Re}[\Sigma_{ii}(0, E_i^{(\lambda)})] = \sum_j \int_0^\infty \frac{\mathrm{d}q}{\pi} \left[\frac{1}{2} \tanh\left(\frac{\xi_q^{\lambda,j} - E_i^\lambda}{2T} \right) [W_{ijji}(q, 0) - V_{ijji}(q)] \right.$$
$$\left. - [W_{ijji}(q, 0) - V_{ijji}(q)] n_B(\xi_q^{\lambda,j} - E_i^\lambda) - W_{inni}(q, 0) n_F(\xi_q^{\lambda,j}) \right]. \tag{15}$$

At zero temperature, the discrete sequence of Matsubara frequencies becomes a continuum, and the frequency sum becomes an integral as $2k_B T \sum \to \int \mathrm{d}\omega / 2\pi$. Furthermore, the Fermi and Bose functions reduce to step functions:

$$n_F(\xi_q^{\lambda,j}) \sim \theta(k_F^\lambda - k_j^\lambda) \qquad n_B(\xi_q^{\lambda,j} - E_i^\lambda) \sim -\theta\left(E_i^\lambda - E_j^\lambda - \frac{\hbar^2 q^2}{2m_\lambda^*} \right) \tag{16}$$

where k_j^λ denotes the wavevector corresponding to the jth subband. The zero-temperature form of the Bose distribution implies that the residue term vanishes for intra-subband interactions whereas it may give a finite contribution for inter-subband terms.

3. Results and discussion

In our numerical calculations, we use the GaAs material parameters, with the effective electron and hole masses respectively taken as $m_e = 0.067m$ and $m_h = 0.4m$, where m is the bare electron mass. We specialize to the zero-temperature calculation to study the density dependence of the BGR within various approximation schemes. Although the finite-temperature case would smooth out the singularities in the integrands, the numerical evaluation was more elaborate, and we did not include this case. Previous studies with the single-subband formulation [9,10] indicate that the renormalization is weakly dependent on temperature in the range ~0–300 K. We believe that including the second subband would not alter this dependence. However, for direct comparison with experimental data, the temperature effects need to be taken into account. In figure 1 we show the subband renormalization as a function of the electron–hole plasma density. The calculation is performed within the fully dynamical RPA formalism for a wire radius of 100 Å and at $T = 0$ K. For these parameters, the second subband starts to populate at $\sim 1.9 \times 10^6$ cm^{-1}, as indicated by an arrow in the figure. There is a significant renormalization of the second subband (dashed line) even before it gets populated. The thin solid line presents the renormalization in the single-subband formulation, to be compared with the thick solid line. For low densities, the two formulations give similar results. As the density increases, and in particular, when the second subband starts to populate, the discrepancy

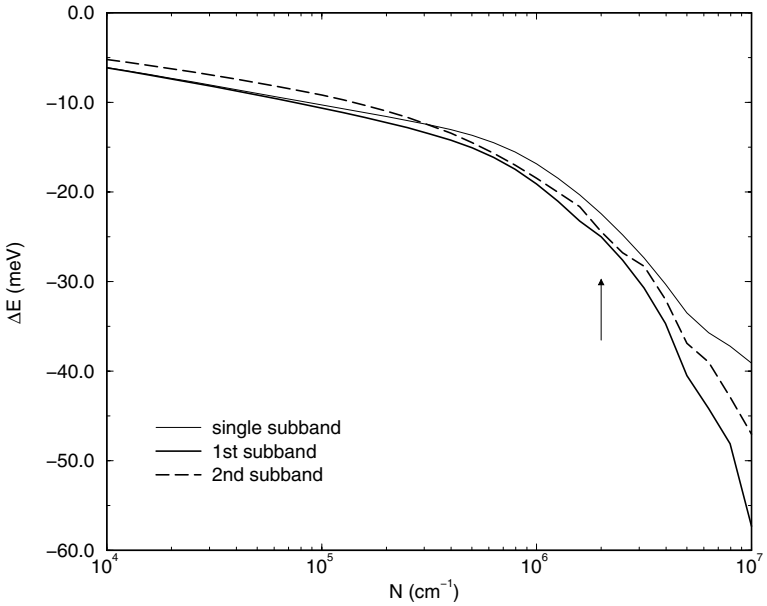

Figure 1. The density dependence of the first-subband (solid line) and second-subband (dashed line) renormalizations of a quantum wire of radius 100 Å, at $T = 0$ K, within the fully dynamical RPA. The thin solid line represents the calculation with the single-subband formulation. The arrow marks the density at which the second subband starts to get occupied, i.e. $N = 1.9 \times 10^6$ cm^{-1}.

between the single-subband and two-subband formulations becomes significant. The multi-subband formulation predicts larger renormalization due to the inter-band contributions. In fact, the very presence of the second subband modifies the renormalization.

The screened exchange and Coulomb-hole contributions to the total renormalization for each subband are shown in figure 2. For low density, the renormalization of the subbands is due to the Coulomb-hole term, but at high density it is carried by the screened exchange term. This is somewhat different to the two-dimensional case [17], where the renormalization is mainly due to the screened exchange term.

In order to gain more insight into the renormalization process in a two-subband system, we plot the intra-subband and inter-subband contributions to the total subband renormalization in figure 3. Referring to the equations (12)–(14), the intra-subband terms have $i = j$, and the inter-subband terms have $i \neq j$. For the first subband (thick lines), the intra-subband contribution dominates the total renormalization, while the inter-subband term starts to contribute significantly with the onset of the second-subband population. Although the second subband (thin lines) has a similar contribution profile for low density, the inter-subband term is more effective, and even exceeds the intra-subband contribution close to the population onset for the second subband. This was anticipated to some extent, as the inter-subband contribution to the second subband comes from the first subband which is filled with carriers.

We have employed the GW-approximation which utilizes the full dynamical RPA dielectric function. A simpler approach is the so-called quasi-static approximation, frequently used in calculations, but the adequacy of this approximation is not well established. In figure 4, we present the BGR calculated within these two approximations. The first indication is that the quasi-static results (the lower pair of curves) tend to overestimate the renormalization for lower densities but, as expected, are close to the full dynamical result in the high-density regime,

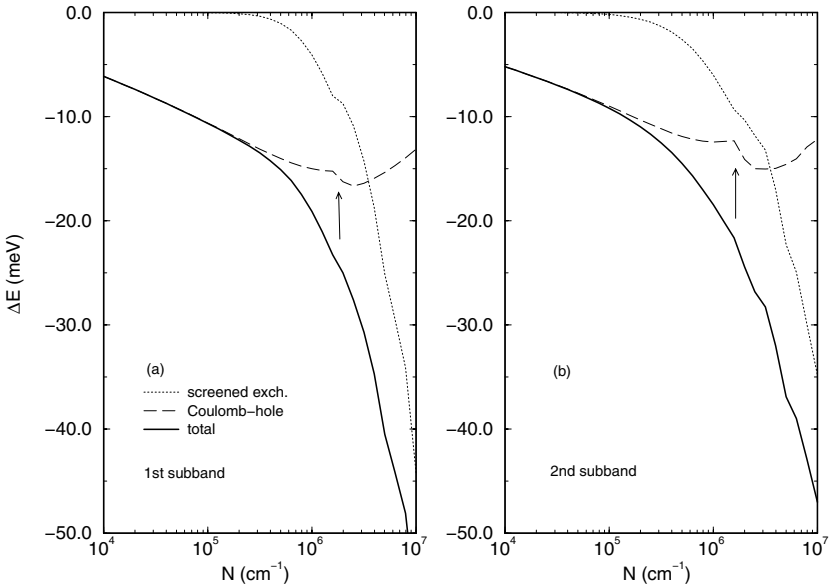

Figure 2. Screened exchange (dotted lines) and Coulomb-hole (dashed lines) contributions to the total subband renormalizations (solid lines) for a quantum wire of radius $R_0 = 100$ Å at zero temperature for the (a) first and (b) second subbands. The arrows mark the density at which the second subband starts to populate.

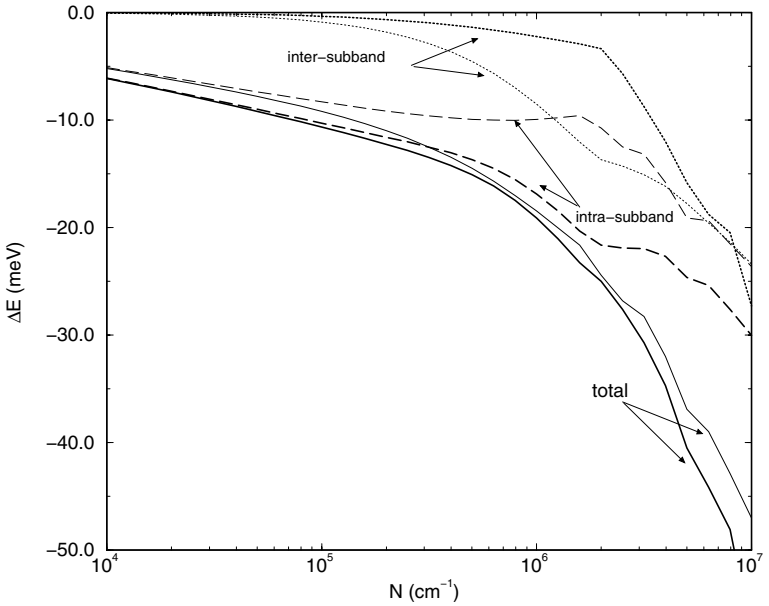

Figure 3. The intra-subband (dashed lines) and inter-subband (dotted lines) contributions to the total subband renormalization (solid lines) in the full RPA. Wire radius $R_0 = 100$ Å. Thick lines are for the first subband and thin lines are for the second subband.

where the RPA itself becomes exact. The dynamical correlations are important in the low-density regime. The renormalization of the second subband suffers from this difference more

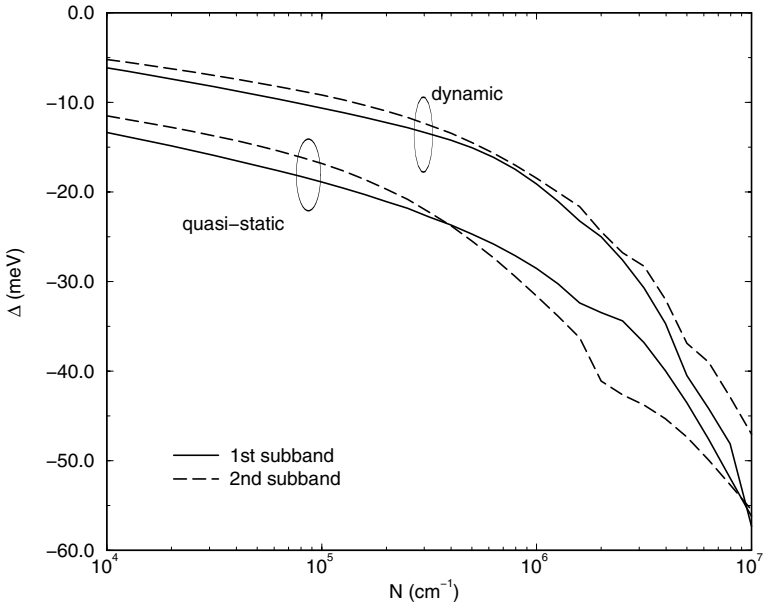

Figure 4. The density dependence of the subband renormalization in the quasi-static (lower pair of lines) and fully dynamical RPA (upper pair of lines) at $T = 0$ K.

severely. As the subband separation is closely related to the wire radius, an investigation of the wire width dependence of the BGR may be interesting for a multi-subband formulation. We plot the radius dependence of the BGR in figure 5 for the fixed plasma densities 1×10^5 cm^{-1}, 1×10^6 cm^{-1}, and 5×10^6 cm^{-1}, from top to bottom, respectively. Within the indicated radius range, these density values correspond to the respective cases where: (a) the second subband is not populated; (b) the second subband starts to populate at around $R_0 = 190$ Å; (c) the second subband is populated throughout the radius range. The renormalization splitting of the subbands is closely related to the wire radius.

3.1. Effects of phonons

The quantum wire structures are fabricated in weakly polar semiconducting materials (e.g. GaAs). In particular, we have shown that the coupling to LO phonons tends to reduce the magnitude of the BGR as compared to the quasi-static approximation results [27]. Similar conclusions have also been reached by Tran Thoai and Cao [28] in their recent work. Here we generalize the formalism previously set out for multi-subband structures to include the phonon effects. In order to include the effects of interaction with phonons, we replace $V_{klmn}(q)$ with $V_{klmn}(q) + V^{ph}_{klmn}(q, \omega)$ in the screened interaction $W_{klmn}(q, \omega)$. For bulk longitudinal optical phonons, the phonon interaction is given by

$$V^{ph}_{klmn}(q, \omega) = \left(1 - \frac{\epsilon_0}{\epsilon_\infty}\right) \frac{\omega^2_{\mathrm{LO}}}{\omega^2 - \omega^2_{\mathrm{LO}}} V_{klmn}(q). \tag{17}$$

Then the total interaction can be written as

$$V_{klmn}(q) + V^{ph}_{klmn}(q, \omega) = \frac{V_{klmn}(q)}{\epsilon(\omega)} \tag{18}$$

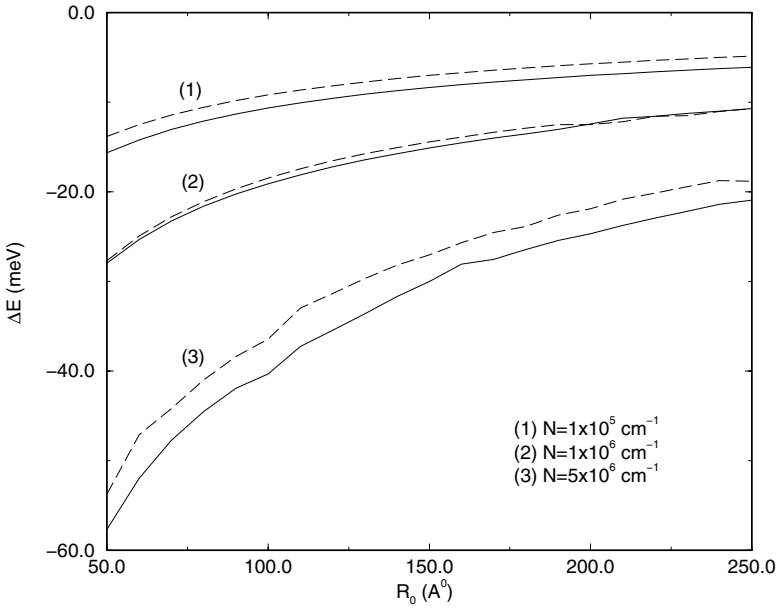

Figure 5. The dependence of the subband renormalization on the wire radius for densities of 1×10^5 cm^{-1}, 1×10^6 cm^{-1}, and 5×10^6 cm^{-1}, from top to bottom, respectively. Solid lines represent the first subband and the dashed lines represent the second subband.

where

$$\epsilon(\omega) = \frac{\omega^2 - \omega_{\mathrm{LO}}^2}{\omega^2 - \omega_{\mathrm{TO}}^2} \tag{19}$$

is the screening function due to the LO phonons. In calculating the BGR in a coupled electron–LO-phonon system, one should subtract the BGR due solely to the phonons which is always present. This polaronic shift is given by

$$\Delta E_i^{ph(\lambda)} = \left(1 - \frac{\epsilon_0}{\epsilon_\infty}\right) \frac{\omega_{\mathrm{LO}}}{2} \sum_n \int_0^\infty \frac{\mathrm{d}q}{\pi}\, V_{inni} \left[\frac{n_B(\omega_{\mathrm{LO}})}{\omega_{\mathrm{LO}} - \xi_q^{\lambda,n}} - \frac{n_B(\omega_{\mathrm{LO}}) + 1}{\omega_{\mathrm{LO}} + \xi_q^{\lambda,n}} \right]. \tag{20}$$

The ϵ_0-approximation consists of replacing ϵ_∞ by ϵ_0 in the effective Coulomb interaction (equation (2)), ignoring the electron–phonon interaction potential ($V^{ph}(q, \omega) = 0$), and adding the polaron shift given above. The main effect of the high-frequency LO phonons is to screen the Coulomb interaction, which is suitably accounted for by the replacement of ϵ_∞ by ϵ_0.

In figure 6 we present the effect due to coupling to LO phonons (solid lines) compared with the ϵ_0-approximation (dotted lines) in the dynamical RPA and the quasi-static approximation for the first subband. Treating the electron–LO-phonon and electron–electron interactions on an equal footing does not affect the full dynamical result significantly; hence the ϵ_0-approximation seems to work well. The dynamical screening function of phonons further decreases the strength of the screened interaction which causes an increase in the renormalization, but then this is compensated by the subtraction of the polaronic self-energy, which brings the renormalization again close to the ϵ_0-result. The quasi-static result, however, is shifted to higher renormalization values, although the subtraction of the polaronic shift tends to reduce it. The net result is that the difference between the quasi-static result and the full RPA increases. In the high-density regime, different approximations merge together, smearing out the polaronic and other dynamical effects.

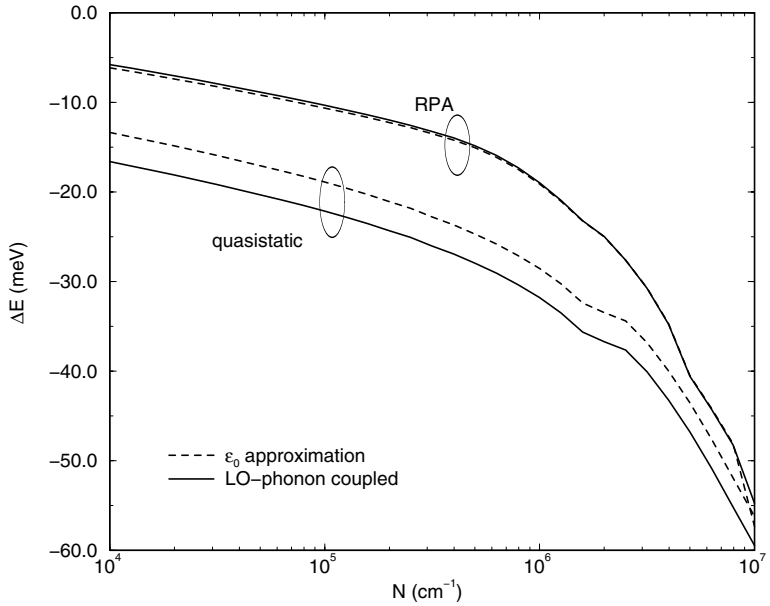

Figure 6. The renormalization of the first subband including the LO-phonon coupling (solid lines) and the ϵ_0-approximation (dashed lines) for the dynamical RPA and quasi-static formulations.

3.2. Vertex corrections

The discrepancies between the RPA-based calculations of the BGR and the measured values have led to the suggestion that the vertex corrections may be important at high densities. In the case of a single-component electron gas, the vertex corrections lead to the $GW\Gamma$-approximation [29] which explicitly includes the vertex function in the self-energy expression and modifies the dielectric function at the same time. The two-component generalization of the above procedure as appropriate to the electron–hole plasma has not been correctly attempted. For two and three dimensions, Shuster, Ell, and Haug [30], by calculating the second-order exchange contribution to the self-energy, have shown that the vertex corrections are quite negligible. It is conceivable that such effects play some role in Q1D systems, and to arrive at a quantitative assessment similar calculations should be performed.

3.3. Validity of the RPA

We have uncritically assumed the validity of the GW-RPA in our calculations reported above, as was done in most other related works [7, 9–12, 14, 28]. Recent work by Moško, Mošková, and Cambel [31] and Moško and Vagner [32] show that the Born approximation to the electron–electron scattering and Lindhard (or RPA) screening are not suitable for Q2D and Q1D structures, suggesting a self-consistent calculation of the Dyson equation (i.e. use of the dressed Green's functions in equation (4)) along with improved approximations to the polarizability may be needed. The RPA employed here should be generally valid for high densities, as the Coulomb coupling parameter $r_s = 1/(2Na_B^*)$ is relatively small. The fully self-consistent calculation of the self-energy is a subject of some debate [33], since the resulting spectral functions typically exhibit spurious satellite structure. Thus, it is not very clear whether a significant improvement may be achieved through the use of the full solution of Dyson's

equation in the high-density range of interest here. As we have mentioned in the previous subsection, the inclusion of vertex corrections implies a better screening function than the Lindhard of RPA counterparts, and it would be interesting to explore their effects in future work. There have been other attempts [34] to calculate the subband renormalization using density-functional theory approaches, with limited success. Recent studies [35] concentrate on the importance of excitonic corrections to the band-gap renormalization in Q1D systems. Generalization of these approaches to multi-subband systems would be necessary to confront experiments.

4. Summary and concluding remarks

In this work, we have considered a fully dynamical treatment of the self-energy and the subband-dependent band-gap renormalization within the RPA for a Q1D electron–hole system. We have taken the dynamically screened Coulomb interaction matrix into account without resorting to approximations. In general, the dynamical correlation effects tend to reduce the magnitude of the BGR, especially as compared to the quasi-static approximation results, and bring the calculated values closer to the experimental ones. Including the second subband in the formulation showed that the very presence of the second subband affects the renormalization even in the absence of occupation by carriers. The multi-subband formulation, however, increases the BGR compared to single-subband case. Our use of the model electron and hole wavefunctions does not pose a serious problem, since the method lends itself to the implementation of numerically calculated more realistic subband wavefunctions if available, which would then lead to a better comparison with the experimental results for a specific wire structure. We chose a quantum wire model with circular cross-section due to the simplicity and ease of calculation of the relevant matrix elements. We stress that, rather than reducing the BGR, we have an increase when the second subband is included. Further work needs to be done in this area, but our main conclusion is that including more subbands in the calculation is not going to produce a smaller BGR. The effects of bulk phonons are also considered. The ϵ_0-approximation seems to work very well compared with the dynamical screening function for phonons within the RPA.

Acknowledgments

This work was partially supported by the Scientific and Technical Research Council of Turkey (TUBITAK) under Grant No TBAG-1662, NATO under Grant No SfP971970, and the Academic Links scheme of the British Council. CRB wishes to thank the Bilkent University Physics Department for hospitality. We also thank Dr G Coli for providing us with preprints of work prior to publication.

References

[1] Sakaki H 1980 *Japan. J. Appl. Phys.* **19** L735
[2] Petroff P M, Gossard A C, Logan R A and Wiegmann W W 1982 *Appl. Phys. Lett.* **41** 635
[3] Demel T, Heitmann D, Grambow P and Ploog K 1988 *Phys. Rev.* B **38** 2732
Christen J, Grundmann M, Kapon E, Colas E, Hwang D M and Bimberg D 1992 *Appl. Phys. Lett.* **61** 67
[4] Cingolani R, Rinaldi R, Ferrara M, La Rocca G C, Lage H, Heitmann D, Ploog K and Kalt H 1993 *Phys. Rev.* B **48** 14 331
Cingolani R, Lage H, Tapfer L, Kalt H, Heitmann D and Ploog K 1991 *Phys. Rev. Lett.* **67** 891
[5] Gustafsson A, Reinhardt F, Biasiol G and Kapon E 1995 *Appl. Phys. Lett.* **67** 3673
Grundmann M 1994 *Semicond. Sci. Technol.* **9** 1939

[6] Schmitt-Rink S, Chemla D S and Miller D A B 1989 *Adv. Phys.* **38** 89
Cingolani R and Ploog K 1991 *Adv. Phys.* **40** 535
[7] Benner S and Haug H 1991 *Europhys. Lett.* **16** 579
[8] Ogawa T and Takagahara T 1991 *Phys. Rev.* B **43** 14 325
[9] Hu B Y-K and Das Sarma S 1992 *Phys. Rev. Lett.* **68** 1750
Hu B Y-K and Das Sarma S 1993 *Phys. Rev.* B **48** 5469
[10] Tanatar B 1996 *J. Phys.: Condens. Matter* **8** 5997
[11] Hwang E H and Das Sarma S 1998 *Phys. Rev.* B **58** 1738
[12] Rinaldi R, Coli G, Passaseo A and Cingolani R 1999 *Phys. Rev.* B **59** 2230
Coli G and Cingolani R 1999 *Solid State Commun.* **110** 293
[13] Wegscheider W 1993 *Phys. Rev. Lett.* **71** 4071
[14] Tassone F and Piermarocchi C 1999 *Phys. Rev. Lett.* **82** 843
[15] Haug H and Schmitt-Rink S 1984 *Prog. Quantum Electron.* **9** 3
[16] Tränkle G, Ell C, Koch S W, Schmidt H E and Haug H 1987 *Phys. Rev.* B **36** 6712
[17] Ryan J C and Reinecke T L 1993 *Superlatt. Microstruct.* **13** 177
Ryan J C and Reinecke T L 1993 *Phys. Rev.* B **47** 9615
[18] For a review see e.g., Cingolani R and Rinaldi R 1993 *Riv. Nuovo Cimento* **16** 1
[19] Ambigapathy R, Bar-Joseph I, Oberli D Y, Haake S, Brasil M J, Reinhardt F, Kapon E and Deveaud B 1997 *Phys. Rev. Lett.* **78** 3579
[20] Gréus Ch, Forchel A, Spiegel R, Faller F, Benner S and Haug H 1996 *Europhys. Lett.* **34** 213
[21] Wang K H, Bayer M, Forchel A, Ils P, Benner S, Haug H, Pagnod-Rossiaux Ph and Goldstein L 1995 *Phys. Rev.* B **53** 10 505
[22] Benner S and Haug H 1994 *Appl. Phys. Lett.* **64** 2824
[23] Gold A and Ghazali A 1990 *Phys. Rev.* B **41** 7626
[24] Li Q P and Das Sarma S 1991 *Phys. Rev.* B **43** 11 768
[25] Hedin L and Lundqvist S 1969 *Solid State Physics* vol 23 (New York: Academic) p 1
[26] Quinn J J and Ferrell R A 1958 *Phys. Rev.* **112** 812
[27] Bennett C R, Güven K and Tanatar B 1999 *Physica* B **263+264** 517
[28] Tran Thoai D B and Cao H T 1999 *Solid State Commun.* **109** 413
[29] Mahan G D and Sernelius B 1989 *Phys. Rev. Lett.* **62** 2718
[30] Shuster S, Ell C and Haug H 1992 *Phys. Rev.* B **46** 16 167
[31] Moško M, Mošková A and Cambel V 1995 *Phys. Rev.* B **51** 16 860
[32] Moško M and Vagner P 1999 *Phys. Rev.* B **59** 10 445
[33] Hedin L 1999 *J. Phys.: Condens. Matter* **11** 489
[34] Godfrey M J and Kubrak V 1995 *Phys. Rev.* B **52** 17 293 (see also reference [17])
[35] Piermarocchi C, Ambigapathy R, Oberli D Y, Kapon E, Deveaud B and Tassone F 1999 *Solid State Commun.* **112** 433
Das Sarma S and Wang D W 1999 *Preprint* cond-mat/9905038
Stopa M 1999 *Preprint* cond-mat/9908349